Herschel/HIFI observations of spectrally resolved methylidyne signatures toward the high-mass star-forming core NGC 6334I

M. H. D. van Der Wiel, F. F. S. van Der Tak, D. C. Lis, T. Bell, E. A. Bergin, C. Comito, M. Emprechtinger, P. Schilke, E. Caux, C. Ceccarelli, et al.

▶ **To cite this version:**

M. H. D. van Der Wiel, F. F. S. van Der Tak, D. C. Lis, T. Bell, E. A. Bergin, et al.. Herschel/HIFI observations of spectrally resolved methylidyne signatures toward the high-mass star-forming core NGC 6334I. Astronomy and Astrophysics - A&A, 2010, 521, pp.L43. 10.1051/0004-6361/201015096 . hal-00633400

HAL Id: hal-00633400
https://hal.science/hal-00633400

Submitted on 30 Nov 2021

HAL is a multi-disciplinary open access archive for the deposit and dissemination of scientific research documents, whether they are published or not. The documents may come from teaching and research institutions in France or abroad, or from public or private research centers.

L'archive ouverte pluridisciplinaire **HAL**, est destinée au dépôt et à la diffusion de documents scientifiques de niveau recherche, publiés ou non, émanant des établissements d'enseignement et de recherche français ou étrangers, des laboratoires publics ou privés.

Distributed under a Creative Commons Attribution 4.0 International License

A&A 521, L43 (2010)
DOI: 10.1051/0004-6361/201015096
© ESO 2010

Astronomy & Astrophysics
Special feature

Herschel/HIFI: first science highlights

Letter to the Editor

Herschel/HIFI observations of spectrally resolved methylidyne signatures toward the high-mass star-forming core NGC 6334I⋆,⋆⋆

M. H. D. van der Wiel[1,2], F. F. S. van der Tak[2,1], D. C. Lis[3], T. Bell[3], E. A. Bergin[4], C. Comito[5], M. Emprechtinger[3], P. Schilke[5,6], E. Caux[7,8], C. Ceccarelli[9,10,11], A. Baudry[10,11], P. F. Goldsmith[12], E. Herbst[13], W. Langer[12], S. Lord[15], D. Neufeld[16], J. Pearson[12], T. Phillips[3], R. Rolffs[6,5], H. Yorke[12], A. Bacmann[9,10,11], M. Benedettini[14], G. A. Blake[3], A. Boogert[15], S. Bottinelli[7,8], S. Cabrit[17], P. Caselli[18], A. Castets[9,10,11], J. Cernicharo[19], C. Codella[20], A. Coutens[7,8], N. Crimier[9,19], K. Demyk[7,8], C. Dominik[21,22], P. Encrenaz[17], E. Falgarone[17], A. Fuente[23], M. Gerin[17], F. Helmich[2], P. Hennebelle[17], T. Henning[24], P. Hily-Blant[9], T. Jacq[10,11], C. Kahane[9], M. Kama[21], A. Klotz[7,8], B. Lefloch[9], A. Lorenzani[20], S. Maret[9], G. Melnick[25], B. Nisini[26], S. Pacheco[9], L. Pagani[17], B. Parise[5], M. Salez[17], P. Saraceno[14], K. Schuster[27], A. G. G. M. Tielens[28], C. Vastel[7,8], S. Viti[29], V. Wakelam[10,11], A. Walters[7,8], F. Wyrowski[5], K. Edwards[30], J. Zmuidzinas[3], P. Morris[3], L. A. Samoska[12], and D. Teyssier[31]

(Affiliations are available on page 5 of the online edition)

Received 31 May 2010 / Accepted 7 July 2010

ABSTRACT

Context. In contrast to the more extensively studied dense star-forming cores, little is known about diffuse gas surrounding star-forming regions.
Aims. We study the molecular gas in the Galactic high-mass star-forming region NGC 6334I, which contains diffuse, quiescent components that are inconspicuous in widely used molecular tracers such as CO.
Methods. We present *Herschel*/HIFI observations of methylidyne (CH) toward NGC 6334I observed as part of the "Chemical *HErschel* Survey of Star forming regions" (CHESS) key program. HIFI resolves each of the six hyperfine components of the lowest rotational transition ($J = \frac{3}{2}-\frac{1}{2}$) of CH, observed in both emission and absorption.
Results. The CH emission features appear close to the systemic velocity of NGC 6334I, while its measured *FWHM* linewidth of 3 km s^{-1} is smaller than previously observed in dense gas tracers such as NH_3 and SiO. The CH abundance in the hot core is $\sim 7 \times 10^{-11}$, two to three orders of magnitude lower than in diffuse clouds. While other studies find distinct outflows in, e.g., CO and H_2O toward NGC 6334I, we do not detect any outflow signatures in CH. At least two redshifted components of cold absorbing material must be present at −3.0 and +6.5 km s^{-1} to explain the absorption signatures. We derive a CH column density (N_{CH}) of 7×10^{13} and 3×10^{13} cm^{-2} for these two absorbing clouds. We find evidence of two additional absorbing clouds at +8.0 and 0.0 km s^{-1}, both with $N_{CH} \approx 2 \times 10^{13}$ cm^{-2}. Turbulent linewidths for the four absorption components vary between 1.5 and 5.0 km s^{-1} in *FWHM*. We constrain the physical properties and locations of the clouds by matching our CH absorbers with the absorption signatures seen in other molecular tracers.
Conclusions. In the hot core, molecules such as H_2O and CO trace gas that is heated and dynamically influenced by outflow activity, whereas the CH molecule traces more quiescent material. The four CH absorbing clouds have column densities and turbulent properties that are consistent with those of diffuse clouds: two are located in the direct surroundings of NGC 6334, and two are unrelated foreground clouds. Local density and dynamical effects influence the chemical composition of the physical components of NGC 6334, which causes some components to be seen in CH but not in other tracers, and vice versa.

Key words. stars: formation – ISM: molecules – ISM: individual objects: NGC 6334I

1. Introduction

Most studies of star-forming regions focus on dense gas in the cores, while much less is known about surrounding diffuse clouds. Methylidyne (CH) can be used as a tracer of low density clouds, since its column density is known to correlate with the total molecular column density in diffuse clouds (Van Dishoeck & Black 1986; Liszt & Lucas 2002; Sheffer et al. 2008; Chastain et al. 2010). In contrast, most carbon is locked in CO in higher density environments ($n(H_2) \gtrsim 10^4$ cm^{-3}), resulting in a lower fractional abundance of CH (e.g., Polehampton et al. 2005).

Interstellar CH was first observed in its electronic transitions in the visual (Adams 1941), and later the Λ-doublet at 3.3 GHz (Rydbeck et al. 1973; Turner & Zuckerman 1974). The accurate determination of a CH abundance from its radio lines is complicated by population inversion effects, while its pure rotational transitions lie in the far-infrared and are unobservable from the ground. While the rotational spectrum of CH has been studied since the 1970s (see Davidson et al. 2001), the first astronomical detection of a rotational transition of CH (at 149 μm) was reported by Stacey et al. (1987) in Sgr B2. With the Heterodyne Instrument for the Far-Infrared (HIFI, de Graauw et al. 2010) onboard the *Herschel* Space Observatory (Pilbratt et al. 2010), it is now possible to observe the ground-state rotational transition of CH at 533 and 537 GHz, free from atmospheric interference and with unprecedented spectral resolution.

⋆ *Herschel* is an ESA space observatory with science instruments provided by European-led Principal Investigator consortia and with important participation from NASA.
⋆⋆ Acknowledgements (page 5) are only available in electronic form at http://www.aanda.org

In this Letter, we study spectrally resolved signatures of the CH $^2\Pi_{3/2}$ J = 3/2–1/2 transition, with an upper level energy of 26 K, toward NCG 6334I, which exhibits emission from the hot core itself, and absorption due to cold foreground clouds. NGC 6334I is a high-mass star-forming core at a distance of 1.7 kpc belonging to the luminous NGC 6334 complex of molecular clouds. The "I" source is composed of several dense subcores (Hunter et al. 2006) with a total mass of ∼200 $M_\odot$ and a bolometric luminosity of several 10^5 $L_\odot$ (Sandell 2000). It is rich in molecular lines (e.g., Schilke et al. 2006). Several foreground clouds have been identified along the line of sight toward NGC 6334 by Brooks & Whiteoak (2001) and Beuther et al. (2005). We use *Herschel*/HIFI data to estimate the CH abundance in the NGC 6334I hot core and constrain the physical properties of the CH absorbing foreground clouds.

2. Observations and data reduction

We use data from a spectral scan from the "Chemical *HErschel* Survey of Star forming regions" key program (CHESS; Ceccarelli et al. 2010), observed by HIFI on board the *Herschel* Space Observatory. The band 1a scan was performed on February 28, 2010 using the dual beam switch (DBS) mode with continuum stability optimization. The half-power beamwidth at the relevant frequencies is about 42″ and was centered at α_{J2000} = 17^{h}20^{m}53^s.32, δ_{J2000} = −35°46′58.5″, which is between the SMA1 and SMA2 cores in Fig. 1 of Hunter et al. (2006). The reference positions for the DBS were ∼3′ east and west of the target. HIFI spectral scans use the wide band spectrometer (WBS) with a frequency resolution of 1.1 MHz, corresponding to 0.6 km s^{-1} at the frequencies of the two groups of CH lines. The full band 1a (480–560 GHz) scan took 12 950 s, including overheads. The resulting noise level is 12 mK in T_{mb} units, measured in 0.5 MHz channels, in the "single sideband" spectrum (see below), averaged between H- and V-polarization. The double sideband system temperature varied between 60 and 110 K.

The raw data is pipelined in HIPE 2.6 (Ott 2010). We note that the absolute velocity scale is uncertain because of improper calculation of the spacecraft motion, but this has been constrained to 0.3 km s^{-1} by subsequent reprocessing in a more recent pipeline version. The resulting level 2 product was processed in CLASS[1]. After mixing the sky signal with a local oscillator (LO) signal, a heterodyne detector such as HIFI yields a double sideband spectrum. In spectral scans, each frequency channel is observed using several LO settings (observations discussed here use a redundancy of 8), which makes it possible to mathematically disentangle the signal from the two separate sidebands (Comito & Schilke 2002). This "deconvolution" step is executed in CLASS, while allowing channel-to-channel variations in receiver gain. Resulting gain variations are 10% at maximum. Spectra presented in this Letter are always deconvolved single sideband spectra. Intensities are corrected for a main beam efficiency of 70.8% expected for band 1a of HIFI.

3. Line profile analysis

The single sideband HIFI WBS spectra near 536.76 and 532.73 GHz (Fig. 1) show continuum emission with T_{mb} = 1.19 K and several spectral lines. The two spectral segments, each about 0.2 GHz wide, cover the CH $^2\Pi_{3/2}$ J = 3/2–1/2 parity $^+$ to $^-$ transitions around 532.73 GHz and the parity $^-$ to $^+$ transitions around 536.76 GHz (Davidson et al. 2001). Most lines are due to CH, but two emission features in the 532.73 GHz spectrum have contributions from the CH_3OH J_K = 15_2–15_1 and the $^{13}CH_3OH$ 9_3–9_2 transitions.

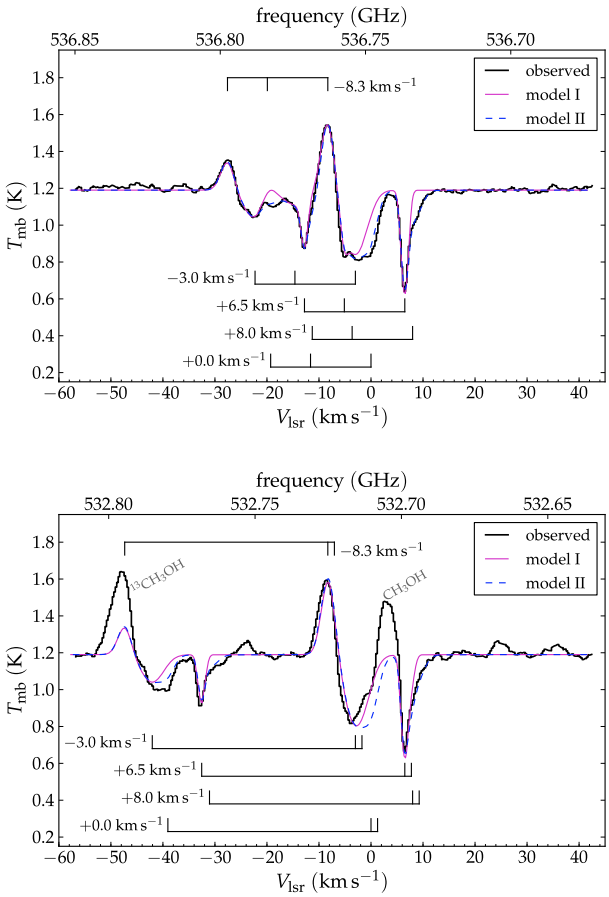

Fig. 1. Observed spectra (black) of the two groups of three hyperfine components of the CH $^2\Pi_{3/2}$ J = 3/2–1/2 transition, represented in T_{mb} units along the vertical axis (see Sect. 2). The horizontal axis gives frequency (*top*) and velocity with respect to the rest frequency for the strongest line in each triplet (*bottom*). The magenta line represents model I with one emission component and two absorption components and the blue line represents model II with two additional absorption components. Physical parameters of the model components are given in Table 1. "Comb" labels indicate the loci of the CH hyperfine lines shifted with respect to the rest frequency.

3.1. Model setup

From inspection of the observed spectrum in Fig. 1, we note that the two sets of three emission peaks are spaced by exactly the hyperfine splitting. Since we see more than three absorption features near each emission triplet, we conclude that more than one absorption component is necessary to explain the observed spectra. We therefore generate a model CH spectrum starting from the minimum of one emitting and two absorbing components ("model I", see Table 1) using the CASSIS software[2] and the CDMS spectroscopic database (Müller et al. 2005). Given an excitation temperature and a column density for a set of emission and absorption lines, the "LTE" module in CASSIS calculates a frequency-dependent optical depth, which is used to construct a beam-averaged, frequency-dependent line brightness.

We adopt a source size of 10″ for the emission component, taken to encompass the four SMA cores (Hunter et al. 2006). With a beam size of 42″ for HIFI band 1a, this results in a beam-filling factor of 6%. Since we lack collisional rate coefficients

[1] Version of April 2010, with some improvements. CLASS is part of the GILDAS software developed at IRAM: http://www.iram.fr/IRAMFR/GILDAS

[2] CASSIS has been developed by CESR-UPS/CNRS (http://cassis.cesr.fr).

Table 1. Model component parameters.

Component	T_{ex} (K)	V_{lsr} (km s^{-1})	$FWHM$ (km s^{-1})	N_{CH} (10^{13} cm^{-2}) model I	model II
Emission	100	−8.3	3.0	20	20
Absorption A	5.5	−3.0	5.0	6.8	6.6
Absorption B	5.5	+6.5	1.5	3.8	3.0
Absorption C	5.5	+8.0	3.5	...	2.1
Absorption D	5.5	+0.0	3.0	...	2.1

for CH, we take the dust temperature of 100 K from Sandell (2000) and assume this to be equal to the excitation temperature (T_{ex}) of the emitting CH gas in NGC 6334I. We note that, while we assume a single value for T_{ex}, the nominal dust temperatures determined from interferometric observations by Hunter et al. (2006) vary between 33 and 100 K from core to core, with limits of 20 and 300 K. The continuum level for the model is fixed at the observed level of 1.19 K. For the absorbing foreground components, T_{ex} = 5.5 K is based on H_2O absorption signatures discussed in Emprechtinger et al. (2010).

3.2. Column density estimates

Since all features in the 536.76 GHz spectrum (Fig. 1, top panel) can be ascribed to CH, we use this as a starting point to constrain the remaining model parameters for the three components: line of sight velocity (V_{lsr}), column density (N_{CH}), and full-width at half-maximum of the line ($FWHM$). The best-fit set of parameters presented in Table 1 (model I) are: emission at V_{lsr} = −8.3 km s^{-1} with $FWHM$ = 3.0 km s^{-1} and $N_{CH} = 2.0 \times 10^{14}$ cm^{-2} and two absorbing components at −3.0 and +6.5 km s^{-1}, with distinctly different line widths of 5.0 and 1.5 km s^{-1}, respectively. After fine-tuning the parameters of the three components, some discrepancies between model I and the observed spectra remain. Extra absorption appears to be required near 536.782, 536.748 and 536.732 GHz (see Fig. 1, top panel). The frequency spacing between these discrepant regions is such that they cannot be explained by a single additional component.

The discrepancies can be resolved by adding two absorbing clouds, both with T_{ex} = 5.5 K and $N_{CH} = 2 \times 10^{13}$: component C with V_{lsr} = +8.0 km s^{-1} and $FWHM$ = 3.5 km s^{-1}, and component D with V_{lsr} = 0.0 km s^{-1} and $FWHM$ = 3.0 km s^{-1} (Fig. 1). Upon introducing components C and D, the column densities of the absorbing components A and B need to be slightly decreased to 6.6×10^{13} and 3.0×10^{13} cm^{-2}, respectively ("model II", Table 1).

Without specific tailoring of the model to match the 532.73 GHz spectrum, it explains this second set of CH signatures remarkably well, with the exception of the contamination by CH_3OH and $^{13}CH_3OH$ (see Fig. 1, bottom panel). Although the addition of components C and D moves the model closer to the spectrum of the 536.76 GHz triplet, the correspondence to the 532.73 GHz spectrum still has some notable discrepancies: the absorption feature near 532.78 GHz is not deep enough, and the absorption signature near 532.72 GHz appears to be shifted by ∼2 km s^{-1}. The latter mismatch could be alleviated by adding a methanol emission line. Additional contamination by other species is not ruled out at the level of ∼0.05 K line intensity, as illustrated by emission features around both 532.670 and 532.754 GHz, and possibly the blue wings of the methanol lines.

3.3. Uncertainties

Variations in column density for an individual model component have a roughly linear effect on the equivalent width of the corresponding spectral feature, i.e., doubling N_{CH} (dividing by two) leads to an emission or absorption line that is twice as strong (weak). Moreover, the column densities that we derive for each component depend directly on the assumed values of T_{ex}. We briefly explore the effect of changing T_{ex} on the line intensities, which we compensate by adjusting the column density. For the emitting gas, raising T_{ex} from 100 to 150 K requires a compensating column density increase of ∼35%, while lowering T_{ex} from 100 to 50 (to 30) K requires a column density decrease of only 20% (15%). Because the CH transition under consideration becomes optically thick at low T_{ex}, the dependence of column density on T_{ex} weakens and eventually reverses as T_{ex} is lowered to ∼50 K and beyond. To illustrate, if T_{ex} is varied from 150 to 100 to 50 to 30 K, the opacity for the main emission line increases from 0.05 to 0.07 to 0.19 to 0.39, respectively. The line opacity therefore reacts more strongly than linearly to a change in T_{ex}, resulting in counterintuitive behavior of line strength as a function of T_{ex}. For the cold absorbing gas, an increase in T_{ex} from 5.5 to 20 K roughly doubles the column density, and changing T_{ex} from 5.5 to 2.7 K results in a column density decrease of <10%. This illustrates a much weaker dependence of column density on T_{ex} than for the emitting gas. Optical depths reach maxima of 0.34, 0.51, 0.15, and 0.18 at the respective line centers for absorbing components A, B, C, and D.

The uncertainty in our derived column density for the emission component is dominated by the uncertainty in the T_{ex} estimates ($\lesssim$2, see Sect. 3.1). Following the above discussion, quoted column density values can be trusted taking into account an error margin of ∼30% for the warm emitting gas. On the other hand, the uncertainty in column densities for the cold absorbing gas components is dominated by measurement errors in the continuum and absorption line depth, each estimated at 6%, resulting in an uncertainty of 8% for the column densities.

4. Discussion

4.1. CH in the hot core

The velocity of the emission component at −8.3 km s^{-1} is consistent with the H_2O emission detected by Emprechtinger et al. (2010) at −8.1 km s^{-1} and close to the velocity of ≈−7 km s^{-1} of molecular lines measured from the ground (Nummelin et al. 1998). The width of the CH emission features of 3.0 km s^{-1} is smaller than the 4–5 km s^{-1} for NH_3 (ATCA at 24 GHz; Beuther et al. 2005), 6.5 km s^{-1} for SiO, and 6 km s^{-1} for HC_3N (IRAM 30m at 87, 130 and 155 GHz; Bachiller & Cernicharo 1990). This difference suggests that the CH emission originates in different, less turbulent and/or less evolved, cores than the heavier N- and O-bearing molecules. Lis et al. (2010) find a similarly narrow linewidth of 3.3 km s^{-1} from HIFI observations of $H^{37}Cl$ 1–0 emission from the NGC 6334I hot core. Sandell (2000) derives a source size of (10 × 8)″ and a dust temperature of 100 K from sub-millimeter dust continuum measurements. Combining this with a 350 μm flux from SHARC-II, dust grain opacities from Ossenkopf & Henning (1994) and the distance of 1.7 kpc, we arrive at $N_{H_2} \approx 3 \times 10^{24}$ cm^{-2}. From this N_{H_2} and our $N_{CH} = 2.0 \times 10^{14}$ cm^{-2}, we find an abundance for CH of 7×10^{-11} relative to H_2 in the hot core. This is a factor ∼7–30 lower than the CH abundance for the dense envelope of Sgr B2, and a factor ∼300 lower than observed CH abundances in diffuse clouds (Polehampton et al. 2005, Table 4, and references therein). This decrease in CH abundance is similar to that predicted by chemical models (Sect. 1) for H_2 densities of $\gtrsim 10^4$ cm^{-3}.

4.2. CH in absorbing clouds

The range of turbulent linewidths for our four absorbing clouds (Table 1) and N_{CH} values of several 10^{13} cm^{-2} agree with models of "turbulence dissipation regions" (Godard et al. 2009)

and with optical observations of diffuse clouds (Liszt & Lucas 2002). Using the range of N_{CH} values for absorption clouds A–D (Table 1) and an N_{CH}/N_{H_2} ratio of 3.5×10^{-8} (Sheffer et al. 2008), we find $N_{H_2} = (0.6–2) \times 10^{21}$ cm^{-2}. Dividing N_{H_2} of 10^{21} cm^{-2} by a number density of 10^2–10^3 cm^{-3} applicable to diffuse gas, we derive a rough linear size estimate of 0.3–3 pc for the absorbing clouds. We also convert $N_{H_2} = (0.6–2) \times 10^{21}$ cm^{-2} into a visual extinction, $A_V \sim 0.3–1$, based on $N_H/A_V = 1.87 \times 10^{21}$ cm^{-2} mag^{-1} (Bohlin et al. 1978). Hence, we conclude that the CH absorption components are diffuse interstellar clouds. We note that, although we discuss several absorbing components as separate entities in velocity space, a diffuse interstellar cloud of several parsecs in size can enjoy a velocity gradient of a few km s^{-1} (cf. *FWHM* in Table 1) and therefore various components may originate in a single molecular cloud.

Other studies also find absorbing gas along the line of sight toward NGC 6334I. We summarize those that potentially correspond to our CH clouds. Brooks & Whiteoak (2001) note two clouds absorbing in OH (near 1.6 GHz) toward several NGC 6334 cores: one cloud with velocities ranging between −15 and +2 km s^{-1}, which they assume to be associated with the NGC 6334 complex, and another at +6 km s^{-1} which they ascribe to a more extended foreground cloud. In addition, the HIFI study of H_2O lines toward NGC 6334I by Emprechtinger et al. (2010) reports absorbing foreground clouds at −6.3, −0.1 and +6.1 km s^{-1}.

In terms of V_{lsr}, our absorption components A and D (Table 1) fit in the widespread [−15, +2] km s^{-1} OH absorption clouds, which places them physically close to the NGC 6334 molecular cloud. In addition, cloud D coincides with one of the three H_2O absorbing clouds. Hence, although N_{CH} for cloud A is three times higher than for cloud D, we conclude that cloud D must be of somewhat higher *number* density to allow for H_2O formation. Moreover, Ossenkopf et al. (2010) find H_2O^+ absorption toward NGC 6334I. There is notable uncertainty regarding the rest frequencies of the H_2O^+ ground state rotational transitions. We assume a value of 1115.209 GHz for $F = 5/2$–$3/2$, which is close to predictions by Mürtz et al. (1998), to derive $V_{lsr} \approx -1$ km s^{-1} for the H_2O^+ absorption. Both the above H_2O^+ signature and the detection of H_2Cl^+ absorption at −1.7 km s^{-1} with a width of 12 km s^{-1} (Lis et al. 2010) are consistent with a blend of our CH components A and D in velocity space.

Our component B at +6.5 km s^{-1} is consistent with both the +6.1 km s^{-1} H_2O absorption (Emprechtinger et al. 2010) and the +6 km s^{-1} OH component to within the 0.7 km s^{-1} velocity resolution of the ATCA observations (Brooks & Whiteoak 2001). We believe that this cloud has a relatively high particle density, but is unrelated to the NGC 6334 complex. Cloud C is seen in CH but has no counterparts in H_2O or OH. The column density of this cloud is not particularly low with respect to clouds A, B, and D (cf. Table 1), but it might simply be of lower number density. In conclusion, from the correspondence with counterparts in other molecules, we find that CH clouds B and C are unrelated foreground clouds, while clouds A and D are located in the direct surroundings of NGC 6334I.

4.3. Dense clouds and outflows

In addition to the absorbing clouds discussed in Sect. 4.2, the literature provides a collection of absorption signatures without CH counterparts. First, we find no evidence of absorbing CH gas that matches the −6.3 km s^{-1} component seen in H_2O (Emprechtinger et al. 2010). The low CH abundance in this cloud – close to the NGC 6334I hot core in velocity space – may be due to its physical proximity to the luminous NGC 6334 region, where higher gas densities facilitate active chemistry, leading to depletion of CH. In general, overall column density and visual extinction are traced more accurately by CH than by H_2O and CO, which are very sensitive to inhomogeneity (e.g., Spaans 1996).

Second, Beuther et al. (2005) detect CH_3OH and NH_3 absorption at 25 GHz toward NGC 6334-I-SMA3 (the compact H II region) at −9 km s^{-1}, about 2 km s^{-1} blueward of the emission component. Moreover, outflows with velocities up to 50 km s^{-1} are observed in H_2O 1_{11}–0_{00}, 2_{11}–2_{02}, 1_{10}–1_{01} and 3_{12}–3_{03} emission (Emprechtinger et al. 2010) and up to 70 km s^{-1} in CO $J = 2$–1, 3–2, 4–3 and 7–6 (Bachiller & Cernicharo 1990; Leurini et al. 2006). In our HIFI observations of the CH transition, we detect neither blueshifted gas nor outflows to match the H_2O, CH_3OH, NH_3, CO and H_2O^+, in neither emission nor absorption. The absence of CH in both blueshifted emission and outflows indicates that CH is destroyed in shocked environments. We conclude that CH traces molecular material that has not yet been swept up by outflow activity related to star formation.

5. Conclusions

We use CH as a tracer of cold, quiescent, molecular gas in both the star-forming core of NGC 6334I and diffuse clouds along the line of sight. We derive a very low CH abundance of 7×10^{-11} in the hot core, consistent with CH depletion in chemically active dense cores. Evidence is found of four absorbing components composed of diffuse gas. From comparison with other molecular absorption signatures in the literature, we conclude that clouds A and D are related to the NGC 6334 complex, and that clouds B and C are unrelated foreground clouds (Table 1). Differences between the four clouds in terms of counterparts in other molecular tracers are ascribed to local variations in density and dynamics. Dynamical stirring of the gas is hypothesized to be the cause of the absence of CH in the outflow component, which *is* detected in other molecular tracers.

References

Adams, W. S. 1941, ApJ, 93, 11
Bachiller, R., & Cernicharo, J. 1990, A&A, 239, 276
Beuther, H., Thorwirth, S., Zhang, Q., et al. 2005, ApJ, 627, 834
Bohlin, R. C., Savage, B. D., & Drake, J. F. 1978, ApJ, 224, 132
Brooks, K. J., & Whiteoak, J. B. 2001, MNRAS, 320, 465
Ceccarelli, C., Bacmann, A., Boogert, A., et al. 2010, A&A, 521, L22
Chastain, R. J., Cotten, D., & Magnani, L. 2010, AJ, 139, 267
Comito, C., & Schilke, P. 2002, A&A, 395, 357
Davidson, S. A., Evenson, K. M., & Brown, J. M. 2001, ApJ, 546, 330
de Graauw, Th., Helmich, F. P., Philips, T. G., et al. 2010, A&A, 518, L6
Emprechtinger, M., Lis, D. C., Bell, T., et al. 2010, A&A, 521, L28
Godard, B., Falgarone, E., & Pineau Des Forêts, G. 2009, A&A, 495, 847
Hunter, T. R., Brogan, C. L., Megeath, S. T., et al. 2006, ApJ, 649, 888
Leurini, S., Schilke, P., Parise, B., et al. 2006, A&A, 454, L83
Lis, D. C., Pearson, J. C., Neufeld, D. A., et al. 2010, A&A, 521, L9
Liszt, H., & Lucas, R. 2002, A&A, 391, 693
Müller, H. S. P., Schlöder, F., et al. 2005, J. Molec. Struct., 742, 215
Mürtz, P., Zink, L. R., et al. 1998, J. Chem. Phys., 109, 9744
Nummelin, A., Dickens, J. E., Bergman, P., et al. 1998, A&A, 337, 275
Ossenkopf, V., & Henning, T. 1994, A&A, 291, 943
Ossenkopf, V., Müller, H. S. P., Lis, D. C., et al. 2010, A&A, 518, L111
Ott, S. 2010, in ADASS XIX, ed. Y. Mizumoto, & M. Ohishi, in press
Pilbratt, G. L., Riedinger, J. R., Passvogel, T., et al. 2010, A&A, 518, L1
Polehampton, E. T., Menten, K. M., Brünken, S., et al. 2005, A&A, 431, 203
Rydbeck, O. E. H., Elldér, J., & Irvine, W. M. 1973, Nature, 246, 466
Sandell, G. 2000, A&A, 358, 242
Schilke, P., Comito, C., Thorwirth, S., et al. 2006, A&A, 454, L41
Sheffer, Y., Rogers, M., Federman, S. R., et al. 2008, ApJ, 687, 1075
Spaans, M. 1996, A&A, 307, 271
Stacey, G. J., Lugten, J. B., & Genzel, R. 1987, ApJ, 313, 859
Turner, B. E., & Zuckerman, B. 1974, ApJ, 187, L59+
Van Dishoeck, E. F., & Black, J. H. 1986, ApJS, 62, 109

Acknowledgements. HIFI has been designed and built by a consortium of institutes and university departments from across Europe, Canada and the United States under the leadership of SRON Netherlands Institute for Space Research, Groningen, The Netherlands and with major contributions from Germany, France and the US. Consortium members are: Canada: CSA, U. Waterloo; France: CESR, LAB, LERMA, IRAM; Germany: KOSMA, MPIfR, MPS; Ireland, NUI Maynooth; Italy: ASI, IFSI-INAF, Osservatorio Astrofisico di Arcetri-INAF; Netherlands: SRON, TUD; Poland: CAMK, CBK; Spain: Observatorio Astronómico Nacional (IGN), Centro de Astrobiología (CSIC-INTA). Sweden: Chalmers University of Technology – MC2, RSS & GARD; Onsala Space Observatory; Swedish National Space Board, Stockholm University – Stockholm Observatory; Switzerland: ETH Zürich, FHNW; USA: Caltech, JPL, NHSC. We thank Marco Spaans for useful discussions, and the referee Volker Ossenkopf for constructive suggestions.

[1] Kapteyn Astronomical Institute, University of Groningen, PO Box 800, 9700AV, Groningen, The Netherlands
e-mail: wiel@astro.rug.nl
[2] SRON Netherlands Institute for Space Research, Groningen, NL
[3] California Institute of Technology, Pasadena, USA
[4] Department of Astronomy, University of Michigan, Ann Arbor, USA
[5] Max-Planck-Institut für Radioastronomie, Bonn, Germany
[6] Physikalisches Institut, Universität zu Köln, Köln, Germany
[7] Centre d'Étude Spatiale des Rayonnements, Université Paul Sabatier, Toulouse, France
[8] CNRS/INSU, UMR 5187, Toulouse, France
[9] Laboratoire d'Astrophysique de Grenoble, UMR 5571-CNRS, Université Joseph Fourier, Grenoble, France
[10] Université de Bordeaux, Laboratoire d'Astrophysique de Bordeaux, Floirac, France
[11] CNRS/INSU, UMR 5804, Floirac Cedex, France
[12] Jet Propulsion Laboratory, Caltech, Pasadena, CA 91109, USA
[13] Ohio State University, Columbus, OH, USA
[14] INAF - Istituto di Fisica dello Spazio Interplanetario, Roma, Italy
[15] Infared Processing and Analysis Center, Caltech, Pasadena, USA
[16] Johns Hopkins University, Baltimore MD, USA
[17] Laboratoire d'Études du Rayonnement et de la Matière en Astrophysique, UMR 8112 CNRS/INSU, OP, ENS, UPMC, UCP, Paris, France
[18] School of Physics and Astronomy, University of Leeds, Leeds UK
[19] Centro de Astrobiologìa, CSIC-INTA, Madrid, Spain
[20] INAF Osservatorio Astrofisico di Arcetri, Florence, Italy
[21] Astronomical Institute "Anton Pannekoek", University of Amsterdam, Amsterdam, The Netherlands
[22] Department of Astrophysics/IMAPP, Radboud University Nijmegen, Nijmegen, The Netherlands
[23] IGN Observatorio Astronómico Nacional, Alcalá de Henares, Spain
[24] Max-Planck-Institut für Astronomie, Heidelberg, Germany
[25] Harvard-Smithsonian Center for Astrophysics, Cambridge MA, USA
[26] INAF - Osservatorio Astronomico di Roma, Monte Porzio Catone, Italy
[27] Institut de RadioAstronomie Millimétrique, Grenoble, France
[28] Leiden Observatory, Leiden University, Leiden, The Netherlands
[29] Department of Physics and Astronomy, University College London, London, UK
[30] Dept. of Physics and Astronomy, University of Waterloo, Canada
[31] European Space Astronomy Centre, ESA, Madrid, Spain